Available online at www.eccomasproceedia.org
Eccomas Proceedia EUROGEN (2023) 245-258

ECCOMAS
Proceedia

EUROGEN 2023
15th ECCOMAS Thematic Conference on
Evolutionary and Deterministic Methods for Design, Optimization and Control
N. Gauger, K. Giannakoglou, M. Papadrakakis, J. Periaux (eds.)
Chania, Crete Greece, 1–3 June 2023

ANALYSIS AND OPTIMIZATION OF PEM FUEL CELLS USING OPENFOAM

Morteza Monfaredi, Evangelos Papoutsis-Kiachagias, Varvara Asouti and Kyriakos Giannakoglou

Parallel CFD & Optimization Unit (PCOpt), School of Mechanical Engineering,
National Technical University of Athens (NTUA), Athens, Greece
e-mail: morteza.monfaredi@gmail.com, {vpapout,vasouti,kgianna}@mail.ntua.gr

Abstract. *In a proton exchange membrane fuel cell (PEMFC), the catalyst layer (CL) and the gas diffusion layer (GDL) are made of porous materials, the characteristics of which affect its performance. The CL determines the ion exchange across the membrane that allows the fuel cell reaction to occur. The GDL transfers the reactant towards the CL and electrons through the solid part, and is important for water management and heat removal. Innovative designs of the porosity distribution in the GDL and CL on both the anode and cathode side, is one of the active research topics in PEMFCs. The optimization presented in this paper redesigns the porosity distribution in the GDL and CL in order to increase the current density and reduce hydrogen consumption. To simulate the PEMFCs, a solver is built in the OpenFOAM environment. This solver performs steady simulations, based on models available in the literature. Results from this analysis tool are verified vs. other numerical results, by comparing the polarization, i.e. the current vs. voltage curve. Here, the evolutionary algorithm-based optimization software EASY of NTUA, which makes use of on-line trained surrogate models to reduce the number of evaluations is used to obtain a front of non-dominated solutions. A bilinear porosity distribution (2D distribution) is used for the GDL along with a uniform distribution for the CL on both the anode and cathode side. It is shown that some of the optimized PEMFC perform better than the baseline one in terms of both performance metrics, with consistent changes along the entire polarization curve.*

Keywords: PEM fuel cell, Porosity Distribution Optimization, Gas Diffusion Layer, Porosity.

Peer-review under responsibility of the organizing committee of EUROGEN 2023.
doi: 10.7712/140123.10203.18935

1 INTRODUCTION

A fuel cell is an electrochemical device that converts the chemical energy of a fuel (such as Hydrogen, H_2) into electricity through a reaction between the fuel and an oxidant. Fuel cells constitute a clean and efficient source of energy as they produce electricity with only water and heat as by-products, unlike traditional power generation methods that release harmful pollutants and greenhouse gases. Proton exchange membrane fuel cell (PEMFC) is a specific variant that uses a polymer electrolyte membrane as the electrolyte. In a PEMFC, H_2 is fed to the anode and Oxygen (O_2) to the cathode, where they undergo an electrochemical reaction to produce electricity, water, and heat [1]. These fuel cells are of interest in a wide range of applications due to their low emissions, high power density and relatively low working temperature [2].

Numerical simulation and optimization techniques are important for the design of PEMFCs; however, their simulation is quite challenging due to the many physics involved in it. Numerical modeling of PEMFCs can be traced back to the work of Springer et al. [3]. Early models were simplistic, based on 1 or 2-D considerations. For example, [4] developed a simplified 2-D, isothermal, single-phase model to study the effect of conductivity, diffusivity, and compression on current density at the interface of the gas diffusion layer (GDL) and the catalyst layer (CL). More sophisticated models are also in use. As mentioned in [5], these mostly differ in the modeling of the water transport in ionomer and two-phase flow, see [6]. The two major types of two-phase models are the two-fluid [7] and mixture [8] ones. The latter, solves the mass, momentum, and species transport conservation equations for the two-phase mixture (liquid water and gas) based on its mass-averaged properties while the former, solves these equations for the gas mixture together with a separate equation for the liquid water transport. Both models are able to accurately predict the PEMFC behavior and are widely used in the literature; the present work makes use of the two-fluid model.

The development of CFD tools for the analysis/simulation of a PEMFC is a continuously evolving field. Some works have used OpenFOAM for this purpose, most of them with simplified models [9, 10, 11, 12]. For instance, in [9] and [10], electrochemical reactions and charge transport equations are not solved; [11] uses a single-phase model and [12] uses an isothermal flow and solves only the flow related equations. In [13], the challenges of increasing power density in PEMFCs are explored, revealing that modifying GDLs is essential as gas diffusivity and thermal conductivity of GDLs have a significant impact on cell performance and durability.

Regarding the optimization of PEMFCs, different methods have been used in the literature to control the structural parameters of a PEMFC stack and working conditions in order to optimize various performance metrics of a PEMFC, such as the current density, power output, energy efficiency and others. In [14], variance analysis, surrogate models, and NSGA-II are combined to optimize the power density, system efficiency, and O_2 distribution of a PEMFC. One of the components that play a significant role in a PEMFC performance is GDL, which is a porous material that not only mechanically supports the membrane electrode assembly (MEA), but also facilitates the transfer of both heat and electrons to the bipolar plate (BP) being in contact with the electrochemically active CL. Therefore, finding the optimal porosity distribution in the GDL is an active research topic [15, 16, 17]. In [15], a gradient-based optimization is used to optimize the constant porosity of the GDL. In [16], the effect of linear porosity distributions on liquid water flux is studied. [17] optimizes a linear porosity distribution in GDL and enhances species transport and current density. The use of a simple (linear or constant) GDL porosity distribution can be justified by manufacturing limitations, [17].

In this paper, a 3D, two-phase model is developed to perform numerical analysis for PEMFCs

and, then, the same tool is used for optimization. This solver is developed in the OpenFOAM environment and results are assessed with respect to (w.r.t.) other published data by comparing the polarization curve. The PEMFC optimization focuses on the porosity distribution in the anode and cathode GDL. The porosity distribution is parameterized using a bilinear function on the x-z plane and kept constant in the y direction, Fig. 1. Here, a two-objective optimization is performed using the evolutionary algorithm-based optimization software EASY of NTUA, employing on-line trained personalized surrogate models to reduce the number of evaluations needed to find the front of non-dominated solutions in the space of two objectives: max. current density at a specific voltage and min. H_2 consumption.

2 MODEL DEVELOPMENT

2.1 Geometry

The structure and dimensions of the PEMFC used herein, Fig. 1, is similar to the one used in [2], the results of which are used, later on, for comparison. This geometry includes the bipolar plate (BP), gas flow channel (GFC), GDL, and CL on both the cathode and anode sides as well as the membrane layer. Due to symmetry, it is enough to consider only the domain of Fig. 1b, discretized with 34800 hexahedral cells.

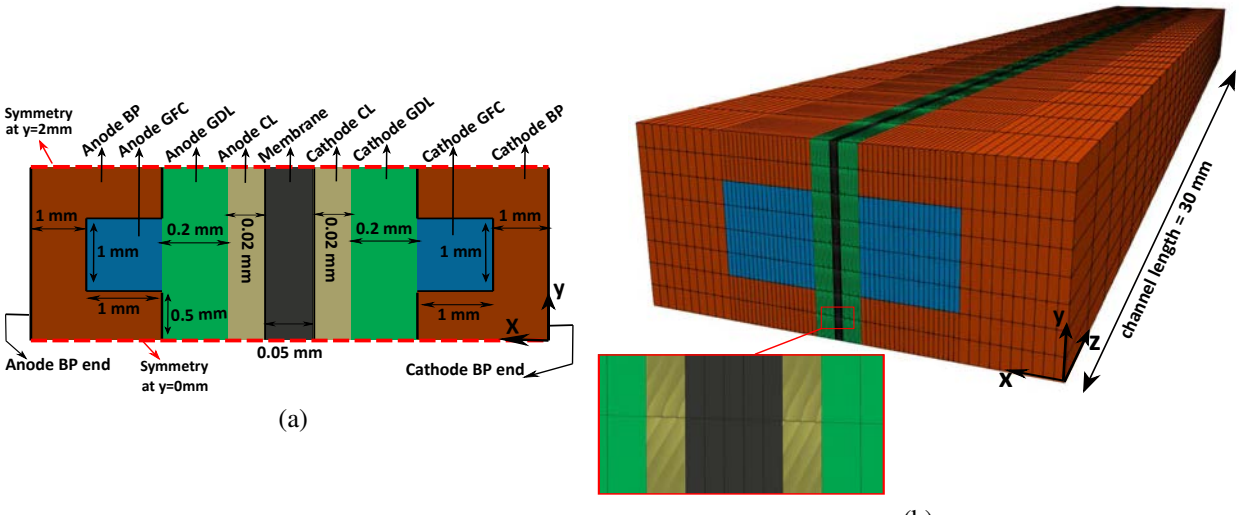

Figure 1: (a) 2D schematic of the PEMFC (not in scale), with dimensions. Dashed black lines at the top and bottom show symmetry. (b) A view of the computational grid; anode and cathode GFC inlets are colored in blue.

2.2 Mathematical Model

The 3D PEMFC simulation makes a steady-flow assumption and relies upon the two-fluid model. The model equations and most of the corresponding assumptions are similar to those frequently used in publications such as [5, 18]. The main assumptions the model makes are that the fluid is laminar and gas mixtures behave as ideal gases; GDL and CL are isotropic and contact resistances between different layers are neglected. Since the model will be used to support optimization runs, two extra assumptions are made to reduce complexity and, thus, computational cost. These assumptions are: (a) water is produced in vapor phase in the cathode

CL, and (b) the fuel cell is working at a constant temperature, thus the energy equation is not solved. The former has been used in some papers such as [5] and the latter can be justified by the fact that the expected temperature change in a PEMFC is relatively low and some models are using physical properties at constant temperature. The governing equations of the model are briefly given below:

The mass conservation equation, which is solved in the fluid domain (GFC, GDL and CL) on both the anode and cathode side, reads

$$\nabla \cdot \left(\rho_g \vec{U}_g\right) = S_m,\ S_m = \begin{cases} -S_{vl} & \text{, GDLs and GFCs,} \\ S_{H_2} - S_{vl} & \text{, anode CL,} \\ S_{O_2} + S_{wv} & \text{, cathode CL.} \end{cases} \tag{1}$$

where S_{vl} is the source due to water evaporation and water vapor condensation, S_{H_2} and S_{O_2} take into account the consumption of H_2 in the anode and O_2 in the cathode, respectively. S_{wv} is the source that accounts for water vapor formation.

The momentum conservation equation for the gas mixture, solved in the same fluid domain, is expressed as

$$\nabla \cdot \left(\frac{\rho_g \vec{U}_g \vec{U}_g}{\varepsilon^2 (1-s)^2}\right) = -\nabla p_g + \nabla \cdot \left(\mu_g \nabla (\frac{\vec{U}_g}{\varepsilon(1-s)})\right) + \vec{S_u},\ \vec{S_u} = -\frac{\mu_g \vec{U}_g}{K} \tag{2}$$

The gas mixture comprises the reactant gases, H_2 and water vapor in the anode and, O_2, N_2, and water vapor in the cathode. The conservation of chemical species equation, solved in the same fluid domain, for the mass fraction of each species y_i (with i being H_2 in the anode, and O_2 and water vapor in the cathode).

$$\nabla \cdot \left(\rho_g \vec{U}_g y_i\right) - \nabla \cdot \left(\rho_g D_i^{eff} \nabla y_i\right) = S_i,\ S_i = \begin{cases} S_{O_2} = \frac{-j_c}{4F} M_{O_2} & \text{, cathode CL,} \\ S_{H_2} = \frac{-j_a}{2F} M_{H_2} & \text{, anode CL,} \\ S_{wv} = -S_{vl} & \text{, anode CL,} \\ S_{wv} = -S_{vl} + \frac{j_c}{2F} M_{H_2O} & \text{, cathode CL.} \end{cases} \tag{3}$$

The mass fractions of N_2 in the cathode and water vapor in the anode are computed since the sum of the mass fractions of all species is equal to 1.

The liquid water transport equation is solved in the same fluid domain and reads

$$\nabla \cdot (\rho_l \frac{K_l \mu_g}{K_g \mu_l} \vec{U}_g) - \nabla \cdot (\rho_l \frac{-K_0 s^3}{\mu_l} \frac{\partial p_c}{\partial s} \nabla s) = S_{vl} \tag{4}$$

The electronic charge (ϕ_{ele}) equation solved in the BPs, GDLs and CLs, and the ionic charge (ϕ_{ion}) equation solved in the CLs and membrane read

$$\nabla \cdot (\sigma_{ele}^{eff} \nabla \phi_{ele}) = S_{ele} \tag{5}$$

$$\nabla \cdot (\sigma_{ion}^{eff} \nabla \phi_{ion}) = S_{ion},\ S_{ele} = -S_{ion} = \begin{cases} j_a & \text{, anode CL} \\ -j_c & \text{, cathode CL} \end{cases} \tag{6}$$

Note that if the expression of a source term in any of the above equations is omitted in a specific domain this implies a zero value there. In the above equations, ρ_g and $\vec{U}_g$ are the density

and velocity of the gas mixture respectively, p_g, ε, s, μ, ϕ_{ele} and ϕ_{ion} are the gas mixture pressure, porosity, liquid water saturation (fraction of the void volume occupied by liquid water), dynamic viscosity, electric and ionic potential, respectively. The rest of the variables with their mathematical expressions are included in table 1 while operational and physical properties of the case are listed in table 2. To solve the above equation, either the operating current density (I) or the PEMFC potential (E_{cell}) must be set and the other results from the simulation. In this study, E_{cell} is set and I is computed by

$$I = \frac{I_a + I_c}{2}, \text{where } I_a = \frac{1}{A_{MEA}} \int_{\Omega_{ACL}} j_a d\Omega \text{ and } I_c = \frac{1}{A_{MEA}} \int_{\Omega_{CCL}} j_c d\Omega \tag{7}$$

where A_{MEA}, Ω_{ACL} and Ω_{CCL} are the electrode active area and the volume of the anode and cathode CL, respectively. Upon convergence, I_c and I_a get almost identical values.

Parameter, symbol	Expression
Molar fraction of species i, x_i	$x_i = \frac{y_i}{M_i} / \sum_j \frac{y_j}{M_j}$
Gas mixture density, ρ_g	$\rho_g = p_g / RT \sum_j \frac{y_j}{M_j}$
Source due to the evaporation/condensation, S_{vl}, [7]	$S_{vl} = \begin{cases} \gamma_{cond}\, \varepsilon\, (1-s) \frac{x_{wv}(x_{wv}p_g - p_{sat})}{RT} M_{H_2O} & x_{wv}p_g > p_{sat} \\ \gamma_{evap}\, \varepsilon\, s\, \rho_l (x_{wv}p_g - p_{sat}) & x_{wv}p_g < p_{sat} \end{cases}$
Saturation pressure, $p_{sat}[atm]$	$log_{10}\, p_{sat} = -2.1794 + 0.02953(T - 273.15)$ $-9.1837 \cdot 10^{-5}(T-273.15)^2 + 1.4454 \cdot 10^{-7}(T-273.15)^3$
Volumetric reaction rate in anode, $j_a[\frac{A}{m^3}]$, [1]	$j_a = (1-s) j_{0,a}^{ref} (\frac{C_{H_2}}{C_{H_2}^{ref}})^{0.5} [exp(\frac{2\alpha_a F}{RT}\eta_{act,a}) - exp(\frac{-2\alpha_c F}{RT}\eta_{act,a})]$
Volumetric reaction rate in cathode, $j_c[\frac{A}{m^3}]$, [1]	$j_c = (1-s) j_{0,c}^{ref} (\frac{C_{O_2}}{C_{O_2}^{ref}}) [-exp(\frac{4\alpha_a F}{RT}\eta_{act,c}) + exp(\frac{-4\alpha_c F}{RT}\eta_{act,c})]$
Anode overpotential, $\eta_{act,a}$	$\eta_{act,a} = \phi_{ele} - \phi_{ion}$
Cathode overpotential, $\eta_{act,c}$	$\eta_{act,c} = \phi_{ele} - \phi_{ion}$
Gas species concentrations, C_i	$C_i = \rho_g y_i / M_i$
Gas phase relative permeability, $K[m^2]$	$K = K_g = K_0 (1-s)^3$
Liquid water relative permeability, $K_l[m^2]$	$K_l = K_0 s^3$
Capillary pressure, $p_c[pa]$	$p_c = \sigma cos\theta \left(\frac{\varepsilon}{K}\right)^{\frac{1}{2}} J(s)$
Leverett function, $J(s)$	$J(s) = \begin{cases} 1.417(1-s) - 2.12(1-s)^2 + 1.263(1-s)^3 & \theta < 90 \\ 1.417s - 2.12s^2 + 1.263s^3 & \theta >= 90 \end{cases}$
Effective diffusivity of species i, $D_i^{eff}[\frac{m^2}{s}]$	$D_i^{eff} = (1 - x_i) / \sum_{j, j \neq i} \frac{x_j}{D_{ij}^{eff}}$
Effective binary diffusivity of component i on component j, $D_{ij}^{eff}[\frac{m^2}{s}]$, [5]	$D_{ij}^{eff} = D_{ij} (\frac{T}{T_{ref}})^{1.5} (\frac{p_{ref}}{p_g}) \varepsilon^{1.5} (1-s)^{1.5}$
Effective electronic conductivity, σ_{ele}^{eff} [7]	$\sigma_{ele}^{eff} = \begin{cases} \sigma_{ele}^{BP} & \text{in BP} \\ (1-\varepsilon)^{1.5} \sigma_{ele}^{GDL/CL} & \text{in GDLs and CLs} \end{cases}$
Effective ionic conductivity, σ_{ion}^{eff} [7]	$\sigma_{ion}^{eff} = \begin{cases} \sigma_i = (0.514\lambda - 0.326)\, exp[1268(\frac{1}{303} - \frac{1}{T})] & \text{in Membrane} \\ [(1-\varepsilon)\varepsilon_{pell}^{Naf}]^{1.5} \sigma_i & \text{in CLs} \end{cases}$
Water activity, a_w	$a_w = x_{wv} p_g / p_{sat} + 2s$
Membrane water content, λ	$\lambda = \begin{cases} 0.043 + 17.81 a_w - 39.85 a_w^2 + 36 a_w^3 & 0 < a_w \leq 1 \\ 14 + 1.4(a_w - 1) & 1 < a_w \leq 3 \\ 16.8 & a_w > 3 \end{cases}$
Nernst potential, E_{Nernst}, [1]	$E_{Nernst} = 1.23 - 0.9 \times 10^{-3}(T - 298) + \frac{RT}{2F} ln(\frac{p_{H_2}}{p_{ref}} (\frac{p_{O_2}}{p_{ref}})^{0.5})$

Table 1: Mathematical expressions associated with the proposed model.

2.3 Boundary Conditions and Numerical Method

At the anode and cathode GFC inlets, the volume flow rate of the inlet gas is fixed which is computed by $Q_{in_{a/c}} = \xi_{a/c}\frac{I_{ref}A_{MEA}}{n_{a/c}FC_{H_2/O_2}}$, where a and c refer to anode and cathode and other variables are given in table 2. Also, Dirichlet conditions are imposed on the liquid water saturation and species mass fractions (which can be computed based on the relative humidity of the inlet gasses) while Neumann conditions are imposed on pressure. At the outlets, pressure is set to the PEMFC working pressure while zero Neumann conditions are imposed on all other variables. At $y=0$ and 2mm (Fig. 1a), symmetry conditions are applied. At the fluid-solid interfaces, a zero Dirichlet condition is imposed on the velocities and zero Neumann conditions on pressure, liquid water saturation and species mass fractions. For the boundary conditions of the electric potential, a zero Dirichlet is set at the cathode BP end-surface. At the anode BP end-surface, the total cell potential loss is imposed, ($\phi_{ele}=E_{Nernst}-E_{cell}$). On the external boundaries, there is a zero flux condition for the ionic potential.

Parameter, symbol	Value	Parameter, symbol	Value
Faraday's constant, $F\ \left[\frac{Coulomb}{mol}\right]$	96485.34	Universal gas constant, $R\ \left[\frac{J}{mol\ K}\right]$	8.314
Condensation rate, $\gamma_{cond}\ \left[s^{-1}\right]$, [7]	1	Evaporation rate, $\gamma_{evap}\ \left[\frac{1}{Pa.s}\right]$	5×10^{-5}
Molar mass of water, $M_{H_2O}\ \left[\frac{g}{mol}\right]$	18.016	Molar mass of H_2, $M_{H_2}\ \left[\frac{g}{mol}\right]$	2.016
Molar mass of O_2, $M_{O_2}\ \left[\frac{g}{mol}\right]$	32	Molar mass of N_2, $M_{N_2}\ \left[\frac{g}{mol}\right]$	28.02
Absolute permeability, $K_0\ \left[m^2\right]$	3×10^{-12}	Reference temperature, $T_{ref}\ [K]$ [5]	333.15
Bulk diffusivity O_2 in water vapor, $D_{O_2-H_2O}\ \left[\frac{m^2}{s}\right]$ [5]	2.82×10^{-5}	Bulk diffusivity O_2 in N_2, $D_{O_2-N_2}\ \left[\frac{m^2}{s}\right]$ [5]	2.2×10^{-5}
Bulk diffusivity water vapor in N_2, $D_{H_2O-N_2}\ \left[\frac{m^2}{s}\right]$ [5]	2.56×10^{-5}	Bulk diffusivity H_2 in water vapor, $D_{H_2-H_2O}\ \left[\frac{m^2}{s}\right]$ [5]	9.15×10^{-5}
Reference pressure, $p_{ref}\ [atm]$ [2]	1	Surface tension, $\sigma\ \left[\frac{N}{m}\right]$ [5]	0.0625
Electronic conductivity of BP, $\sigma_{ele}^{BP}\ \left[\frac{S}{m}\right]$ [2]	8.3×10^4	Electronic conductivity of GDL, $\sigma_{ele}^{GDL}\ \left[\frac{S}{m}\right]$ [2]	5000
Electronic conductivity of CL, $\sigma_{ele}^{CL}\ \left[\frac{S}{m}\right]$ [2]	1000	Volume fraction of nafion in CL,ε_{pell}^{Naf}	0.3
Cathode reference exchange current density, $j_{0,c}^{ref}\ \left[\frac{A}{m^3}\right]$ [5]	120	Anode reference exchange current density, $j_{0,a}^{ref}\ \left[\frac{A}{m^3}\right]$ [5]	5×10^8
Reference molar concentration for O_2, $C_{O_2}^{ref}\ \left[\frac{mol}{m^3}\right]$ [5]	3.39	Reference molar concentration for H_2, $C_{H_2}^{ref}$ $\left[\frac{mol}{m^3}\right]$ [5]	56.4
Anode transfer coefficient, α_a [5]	0.5	Cathode transfer coefficient , α_c [5]	0.5
liquid water contact angle, $\theta\ [degree]$	120	Reference current density $I_{ref}\ \left[\frac{A}{m^2}\right]$	10000
Cathode stoichiometry, ξ_c [2]	2	Anode stoichiometry, ξ_a [2]	1.5
CL porosity, ε_{CL} [2]	0.475	GDL porosity, ε_{GDL} [2]	0.55
n_c	4	n_a	2

Table 2: Data for the baseline case.

The discretization and solution of eqs. 1 to 6 is performed in the open source tool OpenFOAM, using the finite volume method and the SIMPLE algorithm. All equations are solved using the PBiCGStab solver. In each iteration, an inner loop is necessary to make the liquid water equation, eq. 4, converge, due to its high non-linearity. The steps of the solution loop are outlined in Fig. 2.

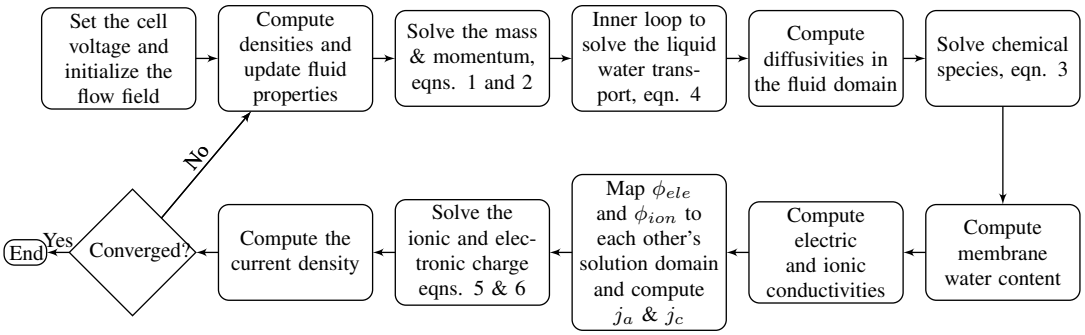

Figure 2: Flow diagram of the solution procedure.

2.4 Code Verification

To verify the software programmed in OpenFOAM, the computed polarization curve is compared with the numerical data of simulation performed by Yuan et. al [2]. As already mentioned, the geometry of the case and most of the physical parameters of the simulation model are the same. Air and H_2 with a relative humidity of 100% are fed to the cathode and anode inlets, respectively. The working temperature and pressure are $343.15K$ and 1 atm, respectively. Comparisons are shown in Fig. 3. A good agreement between the two results can be seen, given that part of the discrepancies is due to the differences [1]in the physical models used. Therefore, the programmed software appears to be ready for running an optimization loop.

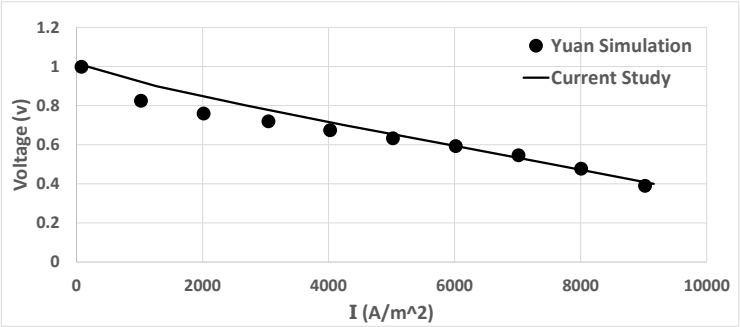

Figure 3: Comparison of the results of the programmed analysis software and numerical data of [2]. In this case, porosity takes on constant values, namely: $\varepsilon_{CL} = 0.475$ and $\varepsilon_{GDL} = 0.55$ at both the anode and cathode.

3 OPTIMIZATION RESULTS

This section describes the optimization of the porosity distribution aiming at maximum current density and minimum H_2 consumption at constant voltage (0.6V). The second objective stands for the difference of the incoming and outgoing H2. This work assumes that unused hydrogen is recirculated to the inlet using a pump and is combined with fresh fuel. When the PEMFC works in recirculation mode, extra actions (such as anode purge to take care of

[1]The main differences are that in [2], a mixture model is used for two-phase flow, the model is nonisothermal and some source term's expression, as well as j_a and j_c formula, are different.

impurities accumulated within the anode) are necessary and, thus, a smart control mechanism (responsible for both the operation of the recirculation pump and the purge valve) is necessary. From a different gas management point of view, such an objective could also be associated with dead-end PEMFC operation too, with the risk of hydrogen dilution, possible carbon corrosion and performance reduction. All these important technical add-ons are beyond the scope of this paper; the interested reader should refer to [19] or other relevant papers. Initially, a parametric study on the porosity effect is performed. Then, the parameterization for the porosity distribution is defined, followed by the optimization run. The obtained results are discussed and compared with those of the baseline (constant) porosity distribution.

3.1 Effect of Porosity - A Parametric Study

Before proceeding to the optimization, the effect of the porosity of the anode and cathode sides on the current density value, at 0.6V, is discussed. To this end, by keeping the porosity on one side constant and equal to that of the baseline ($\varepsilon_{CL} = 0.475$ and $\varepsilon_{GDL} = 0.55$), the other side's CL and GDL porosities vary in the range $[0.1\text{-}0.9]$ with step equal to 0.2. Fig. 4 summarizes the obtained results for both the anode (left) and the cathode (right). In either of them, the current density is more sensitive to the ε_{CL} rather than to the ε_{GDL} value; in practice, the smaller the ε_{CL} the better the results, at least for $\varepsilon_{GDL} \geq 0.3$. The same figure also shows that, for the anode, with a CL porosity value, as the GDL porosity rises, the current density initially remains constant and then reduces. For the cathode, the current density increases first and then decreases. This non-monotonic behavior indicates that there is, indeed, room for optimization.

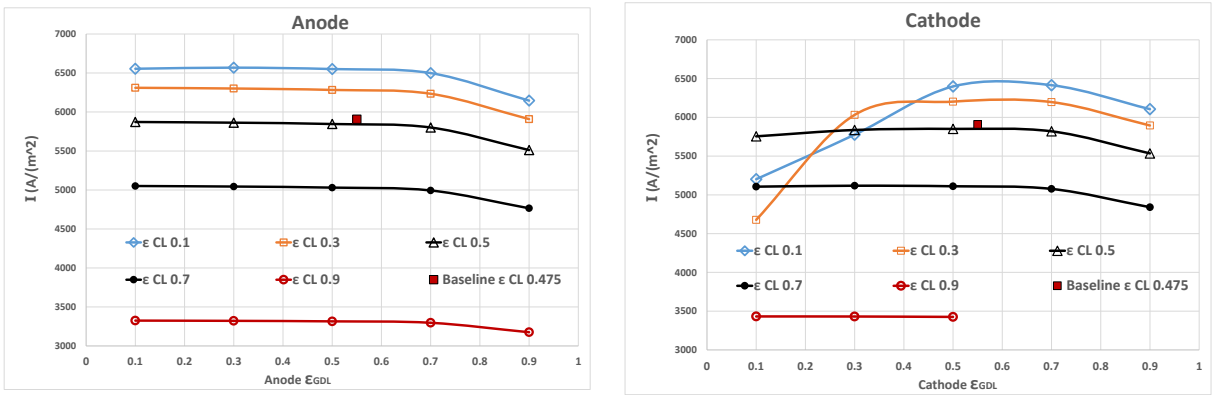

(a) (b)

Figure 4: Effect of the GDL and CL porosity of the (a) anode and (b) cathode side on current density at voltage 0.6V.

3.2 Porosity Parameterization and Optimization Algorithm Set-up

During the optimization, ε_{GDL} and ε_{CL} on both the anode and the cathode sides are allowed to vary. For the CLs, given their small width, a single design variable is used to define the (uniform) porosity on each side. For the GDLs, a uniform distribution along the y direction is assumed while on the x-z plane the porosity follows a bilinear distribution determined by 4 design variables. This results in 5 design variables on each side of the PEMFC or 10 design

variables in total.

The optimization is carried out by means of a metamodel–assisted evolutionary algorithm (MAEA) enhanced by the Principal Component Analysis (PCA). This is implemented in the Evolutionary Algorithms SYstem (EASY) platform, developed by the PCOpt/NTUA. In this work a $(\mu, \lambda) = (10, 18)$ MAEA (with μ parents and λ offspring) is used. The algorithm starts as a standard EA evolving till the first 100 individuals have been evaluated on the PEMFC solver; these are stored in a database and used for building metamodels in all subsequent generations. In specific, personalized metamodels of local validity are used to pre-evaluate each and every new offspring and only a few promising ones (here 2 per generation) are re-evaluated on the PEMFC solver, enriching the database. Cost assignment in the multi-objective problem is carried out by considering dominance and niching criteria; herein the SPEA-2 technique, [20], was used. The PCA is additionally activated after the 3^{rd} generation so as to enhance the MAEA. The PCA, applied to the offspring population, is herein used to control the evolution operators. In specific, the parent population members are transformed into a new feature space with ordered variances (as computed by the PCA). Crossover and mutation are applied in the feature space and the new offspring population is transformed back into the design space. By doing so, the overall optimization algorithm converges faster, as explained in more detail in [21].

3.3 Results and Discussion

As already mentioned, the objective functions are I and H_2 consumption, both defined at 0.6V, to be maximized and minimized, respectively. The baseline case is the one used for code verification with parameter values given in table 2. During the optimization, the design variables are allowed to vary in such a way that the porosity at each and every point at the anode's or cathode's GDL remains within the range of $[0.1\text{-}0.9]$, while for the CL the range is $[0.3\text{-}0.6]$. The max. number of evaluations performed by MAEA is set to 300. The front of non-dominated solutions obtained from the optimization is shown in Fig. 5. At one edge of the front of non-dominated solutions (solution C), a $\sim 25\%$ reduction in the H_2 consumption value is observed which comes with a $\sim 13\%$ less current density. At the other edge (solution A), the current density is increased more than 11% while the H_2 consumption is increased by more than 60%. Of more importance are the solutions such as point B since this outperforms the baseline configuration with respect to both objectives. Below, solutions A, B and C are further discussed.

Comparisons of the porosity distributions between the three selected solutions are plotted in Fig. 6. The lowest porosity of the anode and cathode CL is that of solution A where the CL porosity went down to the lowest allowed value ($\varepsilon_{CL} = 0.3$) whereas the baseline solution has $\varepsilon_{CL} = 0.475$. This is in line with the previous parametric study, which suggests a lower porosity in the CL on both the anode and cathode, for higher current density. This also explains the higher CL porosity for both the anode and cathode sides in solution C. In solution A, in contrast to solutions B and C, the porosity value in most of the anode GDL area is lower than the initial value of 0.55. This implies that, for this case, in the anode side conductivity is playing a more important role, as lower porosity provides better electric conductivity. It can also be seen that in solutions B and C, the cathode GDL porosity is higher close to the outlet area while, on the anode side, the highest porosities are at the inlet. The cathode GDL porosity of solution A changes only in the x direction remaining almost constant in the z direction.

The improved performance of the optimized PEMFCs can also be explained by the contours of the mass fractions of the reactants H_2 in Fig. 7, plotted in the fluid domain (GFC, GDL and CL) of the anode side. As seen, in design C, the mass fraction of H_2 close to the GFC outlet is

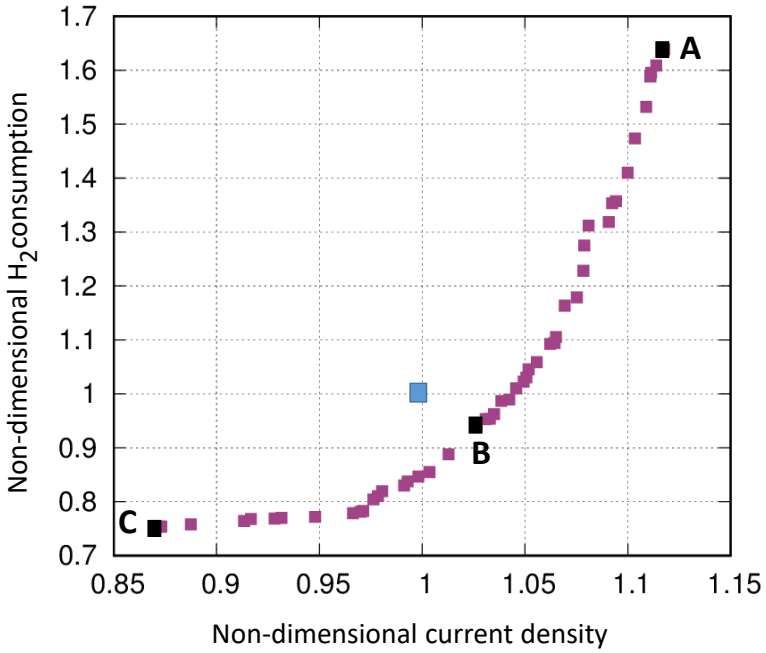

Figure 5: Front of non-dominated solutions obtained from the two-objective optimization run. Values are normalized w.r.t. those corresponding to the baseline PEMFC (blue square). Designs A, B, and C (black squares, to be examined further) belong to the front of non-dominated solutions.

higher than in the other two designs, indicating a lower consumption of reactants in the anode CL. The lowest mass fraction of H_2 can be seen at the outlet of design A with the maximum H_2 consumption. Fig. 8 shows the plots of current density in the cathode CL in the x-z plane at y=1mm; higher values of current density appear in design A.

Though the optimization was carried out at 0.6V, it is also interesting to study the polarization curves of the optimized designs; Fig. 9 compares the polarization curves of the baseline and optimized designs. For designs A and B, an improved polarization performance, compared to the baseline case, can be seen in the entire voltage region although the objective function is defined at a single voltage. As expected, this is not the case for design C. Nevertheless, a consistent behavior in all cases can be seen; in all cases, improving or worsening the current density at one voltage leads to the same behavior at any voltage.

4 CONCLUSIONS

A two-objective optimization of a PEMFC was performed using the EASY software of NTUA that makes use of metamodel-assisted evolutionary algorithms. In a first step, a PEMFC simulation software was programmed in the OpenFOAM environment and is assessed by comparing the numerical results with published data in the literature. Then, a parametric study was performed to overall investigate the effect of porosity on current density which reveals a non-monotonic behavior, particularly in the GDL, emphasizing the importance of optimization. In the optimization, the CL porosities on the cathode and anode side were free to change, by though keeping a uniform distribution, whereas porosity at the GDLs followed a bilinear distribution. The two objectives are the current density and the fuel (H_2) consumption, at a certain voltage. Some designs in the heart of the computed front of non-dominated solutions dominate

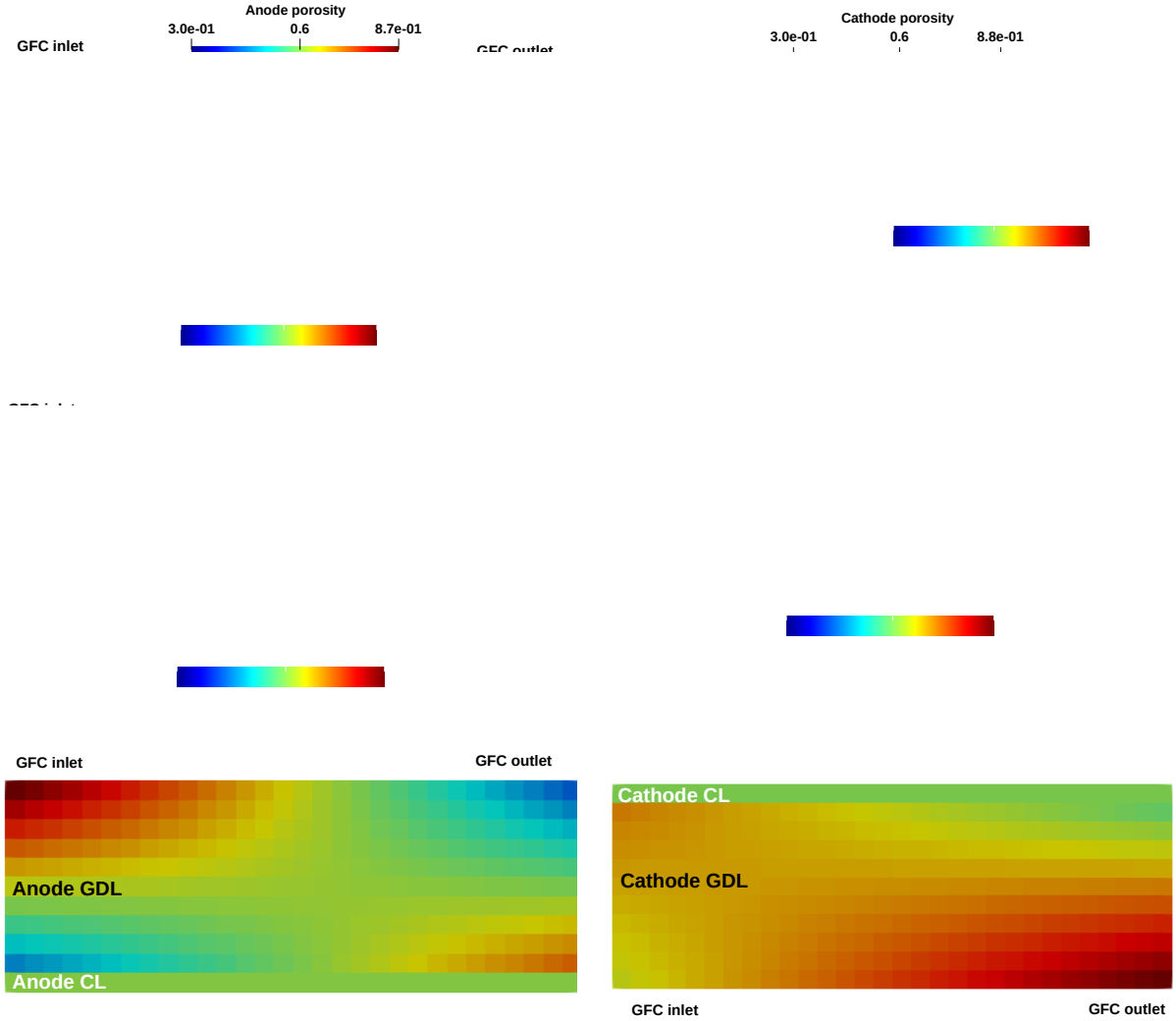

(e) (f)

Figure 6: Porosity distribution in the (left) anode and (right) cathode GDL and CL in the three selected solutions (top) A, (middle) B and (bottom) C. For better visibility, z dimension is scaled. Horizontal and vertical axes correspond to z and x, respectively.

the baseline solution improving both objectives by approximately 5%. Three designs selected from the front are analyzed further. It is important that, even if the optimization took place from a specific voltage, there is a consistent change along the whole polarization curve, in each design.

ACKNOWLEDGMENT

Part of this work was funded by Toyota Motors Europe (TME) and the authors would like to acknowledge Dr. K. Gkagkas for his technical and financial support.

REFERENCES

[1] K. Jiao and X. Li. Water transport in polymer electrolyte membrane fuel cells. *Progress in energy and combustion Science*, 37(3):221–291, 2011.

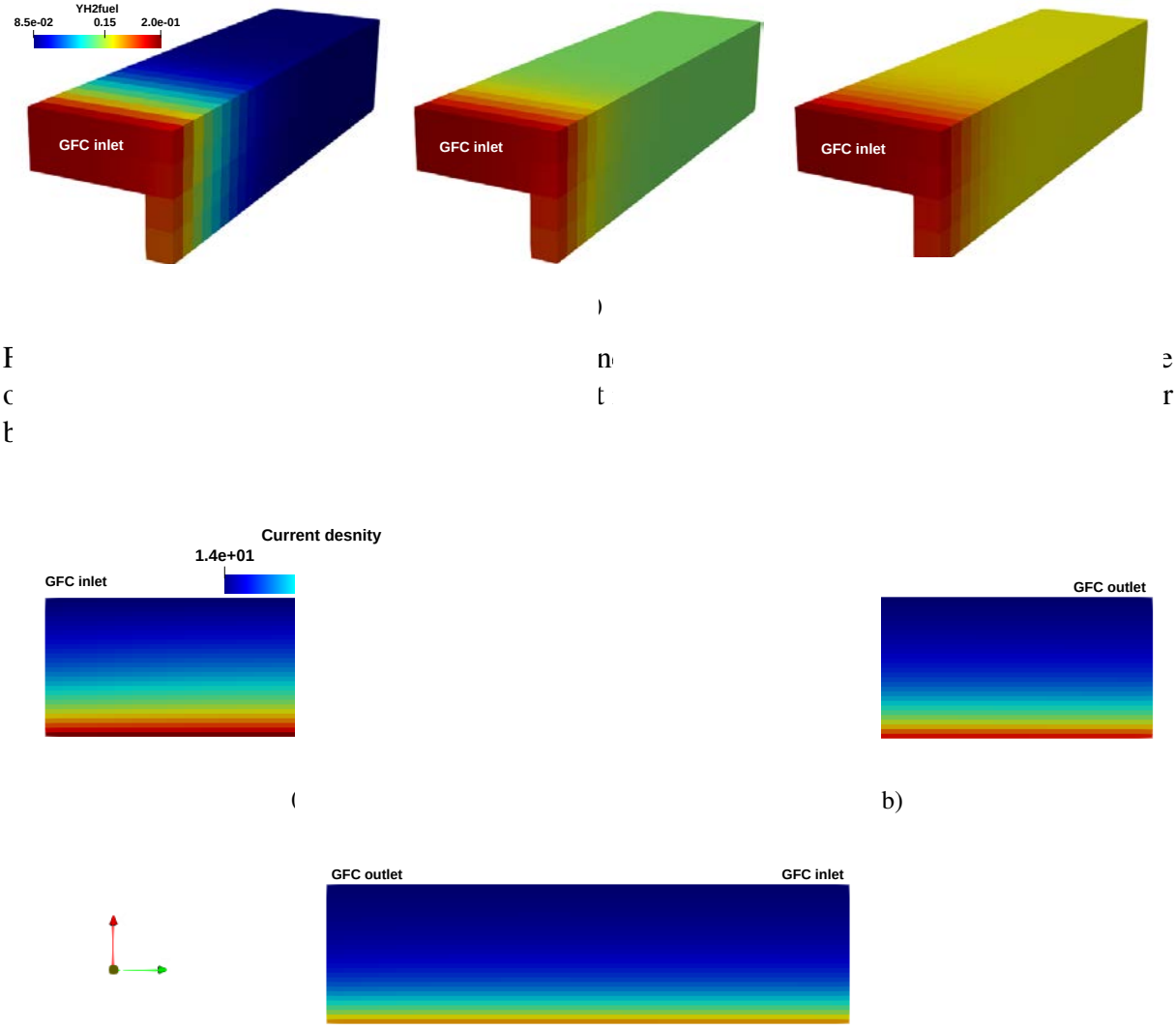

(c)

Figure 8: Contours of current density at x-z plane at half of the height (y=1mm) in cathode CL of the solution (a) A, (b) B and (b) C. For better visibility, z dimension is scaled. Horizontal and vertical axes correspond to z and x, respectively.

[2] W. Yuan, Y. Tang, M. Pan, Z. Li, and B. Tang. Model prediction of effects of operating parameters on proton exchange membrane fuel cell performance. *Renewable Energy*, 35(3):656–666, 2010.

[3] T. E. Springer, TA. Zawodzinski, and S. Gottesfeld. Polymer electrolyte fuel cell model. *Journal of the electrochemical society*, 138(8):2334, 1991.

[4] PC Sui and N Djilali. Analysis of coupled electron and mass transport in the gas diffusion layer of a pem fuel cell. *Journal of Power Sources*, 161(1):294–300, 2006.

[5] H. Wu, X. Li, and P. Berg. On the modeling of water transport in polymer electrolyte membrane fuel cells. *Electrochimica Acta*, 54(27):6913–6927, 2009.

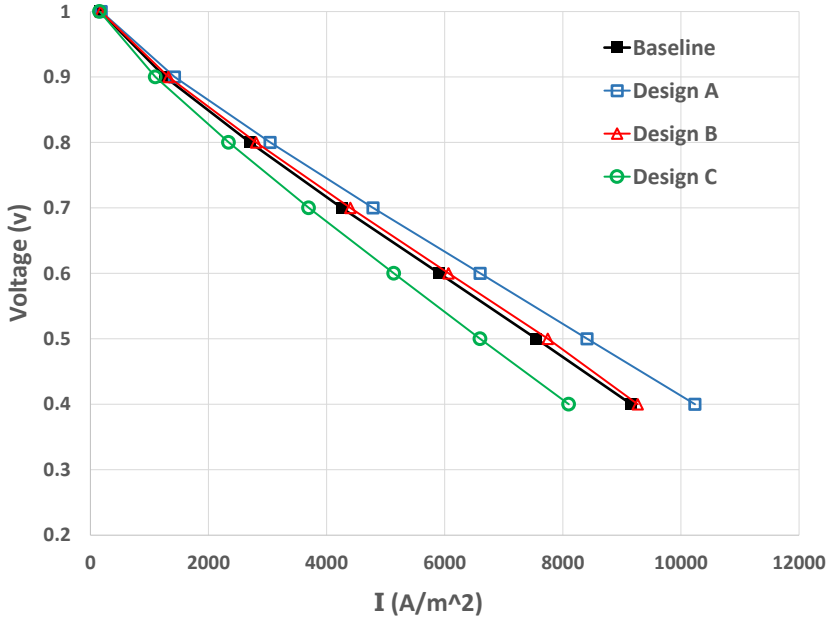

Figure 9: Comparison of the polarization curves between the baseline and optimized PEMFCs.

[6] A. d'Adamo, M. Haslinger, G.e Corda, J. Höflinger, S. Fontanesi, and T. Lauer. Modelling methods and validation techniques for cfd simulations of pem fuel cells. *Processes*, 9(4):688, 2021.

[7] Q. Ye and T. Van Nguyen. Three-dimensional simulation of liquid water distribution in a pemfc with experimentally measured capillary functions. *Journal of the Electrochemical Society*, 154(12):B1242, 2007.

[8] S. Basu, C. Wang, and K. S Chen. Two-phase flow maldistribution and mitigation in polymer electrolyte fuel cells. *Journal of fuel cell science and technology*, 6(3), 2009.

[9] J.P. Kone, X. Zhang, Y. Yan, and S. Adegbite. An open-source toolbox for multiphase flow simulation in a PEM fuel cell. *Comput. Inf. Sci.*, 11(3):10–34, 2018.

[10] JO Ceballos, LC Ordoñez, and JM Sierra. Numerical simulation of a pem fuel cell: Effect of tortuosity parameters on the construction of polarization curves. *International Journal of Hydrogen Energy*, 47(70):30291–30302, 2022.

[11] J. Wang. *Analysis of Deformation of Gas Diffusion Layers and the Impact on Performance of PEM Fuel Cells*. Lund University, 2017.

[12] Z. Niu, Z. Bao, J. Wu, Y. Wang, and K. Jiao. Two-phase flow in the mixed-wettability gas diffusion layer of proton exchange membrane fuel cells. *Applied Energy*, 232:443–450, 2018.

[13] T. Tsukamoto, T. Aoki, H. Kanesaka, T. Taniguchi, T. Takayama, H. Motegi, R. Takayama, S. Tanaka, K. Komiyama, and M. Yoneda. Three-dimensional numerical simulation of full-scale proton exchange membrane fuel cells at high current densities. *Journal of Power Sources*, 488:229412, 2021.

[14] H. Li, B. Xu, G. Lu, C. Du, and N. Huang. Multi-objective optimization of pem fuel cell by coupled significant variables recognition, surrogate models and a multi-objective genetic algorithm. *Energy Conversion and Management*, 236:114063, 2021.

[15] M. Secanell, R. Songprakorp, A. Suleman, and N. Djilali. Multi-objective optimization of a polymer electrolyte fuel cell membrane electrode assembly. *Energy & Environmental Science*, 1(3):378–388, 2008.

[16] Z. Zhan, J. Xiao, D. Li, M. Pan, and R. Yuan. Effects of porosity distribution variation on the liquid water flux through gas diffusion layers of pem fuel cells. *Journal of power sources*, 160(2):1041–1048, 2006.

[17] Y. Huang, C. Cheng, X. Wang, and J. Jang. Effects of porosity gradient in gas diffusion layers on performance of proton exchange membrane fuel cells. *Energy*, 35(12):4786–4794, 2010.

[18] W. Tao, C. Min, X. Liu, Y. He, B. Yin, and W Jiang. Parameter sensitivity examination and discussion of pem fuel cell simulation model validation: Part i. current status of modeling research and model development. *Journal of power sources*, 160(1):359–373, 2006.

[19] H. Lee, H. Su, and Y Chen. A gas management strategy for anode recirculation in a proton exchange membrane fuel cell. *International Journal of Hydrogen Energy*, 43(7):3803–3808, 2018.

[20] E. Zitzler, Laumanns. M., and L. Thiele. SPEA2: Improving the Strength Pareto Evolutionary Algorithm. In *Evolutionary Methods for Design, Optimization and Control with Applications to Industrial Problems, EUROGEN 2001*, Athens, 19-21 September, 2001.

[21] D. Kapsoulis, K. Tsiakas, X. Trompoukis, V. Asouti, and K. Giannakoglou. Evolutionary multi-objective optimization assisted by metamodels, kernel PCA and multi-criteria decision making techniques with applications in aerodynamics. *Applied Soft Computing*, 64:1–13, 2018.